

# Pore fluid pressure diffusion in defluidizing granular columns

Santiago Montserrat, Aldo Tamburrino, Olivier Roche, Yarko Niño

▶ **To cite this version:**

Santiago Montserrat, Aldo Tamburrino, Olivier Roche, Yarko Niño. Pore fluid pressure diffusion in defluidizing granular columns. Journal of Geophysical Research: Earth Surface, 2012, 117 (6), pp.F02034. 10.1029/2011JF002164 . hal-00720261

**HAL Id: hal-00720261**
**https://hal.science/hal-00720261**

Submitted on 20 Oct 2017

**HAL** is a multi-disciplinary open access archive for the deposit and dissemination of scientific research documents, whether they are published or not. The documents may come from teaching and research institutions in France or abroad, or from public or private research centers.

L'archive ouverte pluridisciplinaire **HAL**, est destinée au dépôt et à la diffusion de documents scientifiques de niveau recherche, publiés ou non, émanant des établissements d'enseignement et de recherche français ou étrangers, des laboratoires publics ou privés.

# Pore fluid pressure diffusion in defluidizing granular columns

S. Montserrat,[1,2] A. Tamburrino,[1,2] O. Roche,[3,4,5] and Y. Niño[1,2]

[1] Pore fluid pressure variations play an important role in the motion of natural granular flows like debris and pyroclastic flows. Pore pressure in a defluidizing air-particle bed was investigated by means of experiments and numerical modeling. Experiments consisted of recording the defluidization process, measured as the decay of the basal pore fluid pressure in initially aerated granular mixtures. Mixtures were aerated to different degrees of fluidization by introducing a vertical air flux at the base of a granular column. The degree of fluidization was characterized by the parameter $\beta o$ (pore fluid pressure/lithostatic pressure). Bed expansion occurred for $\beta o > 0.8$–$0.9$, with maximum expansions near 8% at $\beta o \sim 1$. Pore pressure diffusion in our mixtures was modeled by a simple diffusion equation, taking into account a variable diffusion coefficient. When mixtures were expanded ($\beta o > 0.8$–$0.9$), continuous consolidation introduced nonlinearities in the diffusion coefficients, which retarded the decay of pore pressure. In contrast, for non-expanded mixtures, the diffusion coefficient remained constant (linear diffusion). Our results highlight that mixture compressibility can effectively reduce the pressure diffusion coefficient in initially expanded granular mixtures, thus increasing the duration of pressure diffusion. In our experiments, as well as for most self-consolidating natural granular mixtures, changes in permeability due to mixture consolidation appear to be negligible for the defluidizing process, as they are counteracted by changes in porosity and because the fluid behaves as incompressible, even when the fluid is air.

## 1. Introduction and Objective

[2] Geophysical granular flows consist of solid-fluid mixtures driven by gravity, which propagate over natural terrains. The solid phase typically consists of grains of different sizes, commonly ranging from microns to decimeters and possibly meters, while the fluid phase is either water or gas. In case of water-solid mixtures, fine sediments and water act as an equivalent fluid phase, with a different effective fluid viscosity, and possibly rheology, with respect to pure water [*Iverson*, 1997; *Major*, 2000]. Examples of geophysical granular flows include debris flows, pyroclastic flows, snow avalanches, and rock avalanches [*Iverson*, 1997; *Iverson and Denlinger*, 2001; *Jain et al.*, 2004; *Freundt et al.*, 2000]. Since *Bagnold* [1954] introduced the concept of dispersive stress, important advances have been made regarding the understanding of fluid-particle flow dynamics. Nevertheless, the formulation of general constitutive laws and their relation with mixture constituents and terrain characteristics remains an active research field.

[3] Geophysical granular flows have been commonly modeled using shallow water equations to solve their bulk behavior [*Savage and Hutter*, 1989; *Denlinger and Iverson*, 2001; *Iverson et al.*, 2004; *Vollmöller*, 2004; *Pudasaini et al.*, 2005]. A major issue arises when considering an appropriate flow resistance relationship to adequately describe the flow regime. Such flows have often been modeled as plastic materials, and two plastic theories are commonly used: viscoplasticity and Coulomb plasticity. A viscoplastic model often assumes an equivalent single-phase viscous fluid with a specific rheology, typically of Bingham or Herschel-Bulkley type, as considered in pure fluid mechanics [*Ancey*, 2007; *Naef et al.*, 2006]. In contrast, Coulomb plasticity derives from soil-mechanics considerations. Coulomb models are two-phase models that consider both a solid and a fluid phase. The fluid-phase energy dissipation is commonly treated as a viscous term, while inter-particle interactions are assumed to be dominated by friction, which is well described by the Coulomb law [*Savage and Hutter*, 1989; *Iverson*, 1997; *Iverson and Denlinger*, 2001; *Savage and Iverson*, 2003; *Iverson et al.*, 2004; *Hutter et al.*, 2005; *Pudasaini et al.*, 2005; *Ancey*, 2007]. Inter-particle

[1]Departamento de Ingeniería Civil, Universidad de Chile, Santiago, Chile.
[2]Advanced Mining Technology Center, AMTC, Universidad de Chile, Santiago, Chile.
[3]Clermont Université, Université Blaise Pascal, Laboratoire Magmas et Volcans, Clermont-Ferrand, France.
[4]UMR 6524, LMV, CNRS, Clermont-Ferrand, France.
[5]IRD, LMV, Clermont-Ferrand, France.

Corresponding author: S. Montserrat, Departamento de Ingeniería Civil, Universidad de Chile, Avda. Blanco Encalada 2002, Santiago, Chile. (smontser@ing.uchile.cl)

friction is controlled by pore fluid pressure, which counterbalances the weight of the particles, thus reducing contact shear stresses according to the Terzaghi effective-stress principle [*Iverson*, 1997; *Iverson and Denlinger*, 2001; *Savage and Iverson*, 2003; *Goren et al.*, 2010]. Thus, intergranular pore fluid pressure appears important for understanding the dynamics and mobility of granular flows. When dilute mixtures are highly agitated, particle collisions dominate energy dissipation within the flow. In these cases, constitutive equations derived from the kinetic theory of gases have provided good flow descriptions [*Campbell*, 1990; *Azanza et al.*, 1999; *Goldhirsch*, 2003]. In most natural granular flows, as well as in industrial applications, the two limiting regimes, frictional and collisional, coexist [*Ancey and Evesque*, 2000; *Armanini et al.*, 2005]. Two-dimensional numerical simulations of sheared granular layers have shown the appearance of force chains, formed by long-lasting contact networks (frictional forces), which transmit most of the stress within the flow [*Aharonov and Sparks*, 1999]. Vertical rheological stratification has been experimentally observed by *Armanini et al.* [2005, 2008] in chute flows, where distinct sub-layers are characterized by either frictional or collisional regimes.

[4] Observations made at different scales support the idea that pore fluid pressure in excess of hydrostatic or atmospheric pressure, respectively, in wet and dry mixtures (hereafter named excess pore fluid pressure), can be retained for long durations. High pore fluid pressure has been measured in experimental and natural debris flows [*Iverson*, 1997; *Major and Iverson*, 1999; *McArdell et al.*, 2007] and in laboratory experiments on initially fluidized air-particle flows [*Roche et al.*, 2010], and explains why the run-out of fluidized flows can be twice that of non-fluidized flows [*Roche et al.*, 2004, 2008; *Girolami et al.*, 2008]. In spite of the prevailing idea that differential fluid-particle motion generates excess pore fluid pressure that may diffuse in ways that depend on the mixtures characteristics [*Iverson and LaHusen*, 1989; *Iverson*, 1997; *Iverson and Denlinger*, 2001; *Goren et al.*, 2010, 2011], the details of the associated pore pressure dynamics (generation, transport and diffusion) are still poorly understood. Based on experimental data, *Iverson and Denlinger* [2001] proposed that basal pore pressure should advect passively with the flow in the horizontal directions ($x$ and $y$) and simultaneously diffuse in the vertical direction ($z$) following a simple linear diffusion model [*Iverson and Denlinger*, 2001, equation 59]. This approach has been used by different authors to model debris flows and has led to good results, requiring a prescribed model for the pore pressure diffusion coefficient [*Vollmöller*, 2004; *Denlinger and Iverson*, 2001; *Pudasaini et al.*, 2005]. *Savage and Iverson* [2003] explicitly coupled a pore pressure-diffusion equation to changes in debris flow thickness and showed that pore pressure can be generated due to changes in flow height. Recently, a numerical model coupling the evolution of dilatancy, solid and fluid volume fractions, pore fluid pressure, and flow depth and velocity has demonstrated the ability to simulate debris flows from initiation to deposition [*George and Iverson*, 2011]. Numerical results compared well with experimental data.

[5] Previous one-dimensional experimental results on a defluidizing static column have shown that above a critical value of about ~80–90% of full initial fluidization, occurring at the onset of bed expansion, the pore pressure diffusion coefficient drops abruptly. Linear pore pressure diffusion models [*Major*, 2000; *Iverson and Denlinger*, 2001] fail to represent the pore pressure diffusion in static granular columns for fluidization degrees exceeding those triggering the onset of bed expansion [*Montserrat et al.*, 2007]. At the same critical fluidization threshold, an important increase in the run-out distance of initially expanded mixtures occurs [*Montserrat et al.*, 2007; *Roche et al.*, 2004, 2008, 2010], suggesting that changes in the pore pressure diffusion dynamics may significantly affect flow behavior. This work aims to extend the present understanding of pore pressure diffusion at fluidization degrees exceeding the critical value, for expanded mixtures, toward a better description of the implications and modeling of pore pressure in granular flows. To this purpose, we carried out coupled experimental and numerical studies on the pore pressure diffusion process in a static granular bed. Experiments focused on the decay of pore pressure at the base of a reservoir filled with an air-particle mixture that can be fluidized at different degrees by introducing a vertical upward air flux through the granular medium [*Montserrat et al.*, 2007]. Similar, fluidization techniques have been used since the early 1970s in studies related to industrial applications as well as to pyroclastic flows [e.g., *Davidson and Harrison*, 1971; *Geldart*, 1973; *Wilson*, 1980; *Geldart and Wong*, 1985; *Lorences et al.*, 2003; *Roche et al.*, 2004, 2008, 2010; *Druitt et al.*, 2007]. In our experiments, fluidization was used to generate an initial excess pore pressure gradient, above atmospheric, within the granular mixture. In nature, excess pore fluid pressure can be caused by particle settling or by the presence of an upward fluid flux, both configurations being dynamically equivalent [*Richardson and Zaki*, 1954; *Druitt et al.*, 2007]. Our results show that pore pressure diffusion can be well represented, from nil to complete fluidization, by a simple linear diffusion model taking into account a variable diffusion coefficient. The coefficient is a strong function of the mixture compressibility, which in turns depends on the initial degree of fluidization. For low degrees of fluidization, the linear diffusion model (with a constant pore pressure diffusion coefficient) is recovered.

[6] The experiments presented here are probably the simplest way to study pore pressure diffusion in granular mixtures, and represent a first step toward the study of pore pressure in flowing mixtures. We acknowledge that in sheared flows, however, complex processes such as deposition, varying flow height [*Girolami et al.*, 2008; *Roche et al.*, 2010], continuous grain rearrangement (dilative-compactive grains motion [*Iverson and LaHusen*, 1989; *Goren et al.*, 2010]), self-fluidization due to flow instabilities and gas entrainment [*Bareschino et al.*, 2008], and other processes can affect pore pressure dynamics.

## 2. Experimental Device and Procedure

[7] The experimental device (Figure 1) consisted of a 0.5 m tall rectangular Plexiglas reservoir having a cross-sectional area of $0.1 \times 0.2$ m$^2$, which contained a dry particle mixture. An air flux was introduced through a 10 mm

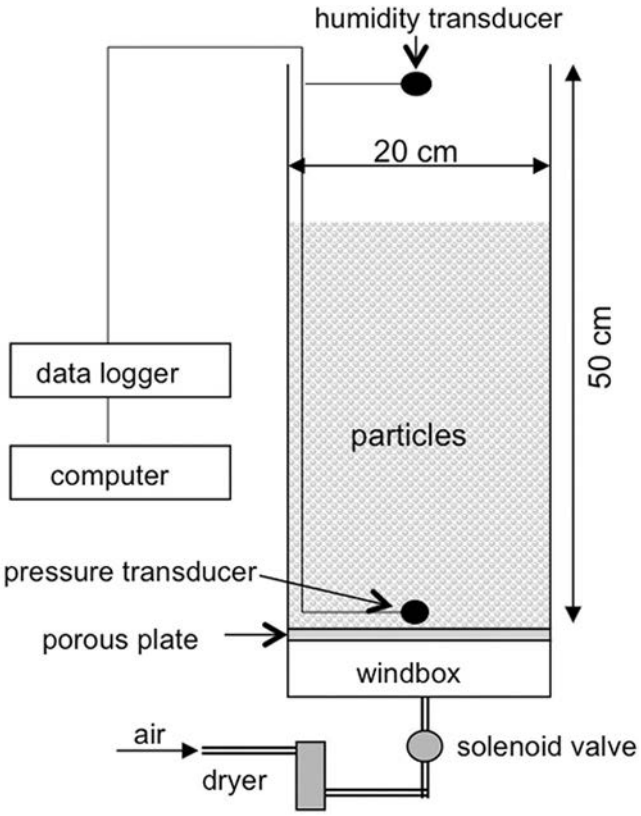



**Figure 1.** Sketch of the experimental device.

thick porous plate (pore size ~20 $\mu$m) located at the bottom of the reservoir in order to fluidize the mixture. Air was first introduced in a wind box separated from the tank by the porous plate (Figure 1). A pressure transducer, placed perpendicular to the upward air flux, continuously measured the pore pressure at the base of the reservoir. Airflow velocities (with maximum interstitial values ~10 mm/s) were low enough to not affect the pressure transducer readings. The air flux could be stopped almost instantaneously (in ~0.01 s) by means of a solenoid valve, thus starting the defluidizing process. Pore pressure could not diffuse back toward the porous plate because pressure was maximum in the wind box. Measurements taken inside the wind box showed that pressure diffused almost instantaneously (<0.01 s) when no particles were placed above the porous plate. Thus, the wind box could be neglected in the analysis, and the porous plate could be assumed as an impermeable wall above the granular column after the solenoid valve was closed. Therefore, pore pressure diffusion only occurred in the upward direction. Special care was taken to control the mixture humidity in order to avoid excessive cohesion and electrostatic effects and to ensure reproducibility of the experiments. Air was dried before entering the reservoir. A humidity transducer placed at the top of the reservoir controlled the air flux relative humidity (RH), which had a mean value of 35% ± 5%. Before each experiment, the particles were aerated for about one hour.

[8] When a vertical airflow is supplied at the bottom of a granular column, an upward drag force is exerted on the particles. When the drag force is less than the weight of the particles, the granular column is commonly termed aerated [*Gibilaro*, 2001]. If the weight of the particles is fully counterbalanced by the drag force, the column is termed fluidized. In fluidized granular columns, intergranular frictional stress is negligible and the fluid-particle mixture acquires fluid-like properties, with the internal pore fluid pressure equaling that generated by the particle network. A linear pressure gradient is established during the aeration procedure, with maximum pore pressure at the base of the mixture and atmospheric pressure at the top of the granular column. The degree of fluidization is defined by comparing the pore pressure at the base of the granular column ($p_{bed}$) with the lithostatic pressure, $P_L$, (defined as the particles weight divided by the cross-sectional area of the container). Thus, when $p_{bed}/P_L = \beta_0 < 1$, the bed is aerated, and when $p_{bed}/P_L = \beta_0 = 1$, the bed is fully fluidized.

[9] We used nearly spherical glass beads, with a density of 2500 kg/m$^3$ (Ballotini, Potters Industries), which had almost the same characteristics as those used by *Roche et al.* [2004, 2008, 2010] in their dam break studies on air-particle flows. Particle diameter ranged from 45 to 90 $\mu$m, with a mean diameter of about 60 $\mu$m (measured by a Mastersizer 2000 particle analyzer, Malvern Instruments Ltd.). The bulk density of the granular bed was 1400 ± 40 kg/m$^3$, which indicated a porosity of 0.44 ± 0.02. In terms of their gas fluidization properties, the particles belonged to the *Geldart* [1973] group A. This means that once particles are fully fluidized at a critical airflow velocity, *Umf* (minimum fluidization velocity), gas bubbles form at a second critical velocity, *Umb* > *Umf*. Note that airflow velocity is defined as the volumetric airflow rate (introduced at the bottom of the reservoir) divided by the reservoir cross-sectional area. Between *Umf* and *Umb*, the homogeneously fluidized bed expands linearly as the flow rate is increased [*Gibilaro*, 2001; *Roche et al.*, 2004]. In practice, fluidization may not be fully homogeneous throughout the granular column, as airflow channeling tends to occur. Thus, bed expansion may occur before complete fluidization is achieved [*Gilbertson et al.*, 2008]. For this reason, *Umf* is defined in practice as the air velocity at the onset of bed expansion, which commonly occurs at velocity slightly smaller than that for which full bed support is achieved. This definition is used here [cf. *Roche et al.*, 2004; *Druitt et al.*, 2007].

[10] At the laboratory scale, the use of group A particles of small grain size (and hence small permeability) is required for allowing pore pressure measurements, as mixtures of coarser particles diffuse pore pressure too fast and are almost immediately defluidized [*Iverson*, 1997; *Major*, 2000; *Iverson and Denlinger*, 2001, *Druitt et al.*, 2007, *Roche et al.*, 2004]. It is important to note that our experiments best apply to natural gas-particle mixtures, such as pyroclastic flows, because fluidized beds of pyroclastic debris that consist of a matrix of fine ash have a typical group-A behavior, including homogenous expansion [*Druitt et al.*, 2007]. In addition, the defluidization process characteristics of our beds of group-A particles share similarities with pore pressure diffusion in consolidating debris flow deposits [*Iverson*, 1997; *Major*, 2000]. In particular, *Major* [2000] showed experimentally that pore fluid pressure in debris flow deposits can diffuse in a few seconds to several

hours depending on the amount of fine sediment in the debris.

## 3. Pore Pressure Modeling

[11] The complete equation describing the dynamics of pore pressure in porous media is well known and can be easily derived by coupling the fluid-phase continuity equation (equation (1)) with the Darcy equation (equation (2)), which is a reduced form of the fluid-momentum equation assuming negligible inertia [*Goren et al.*, 2010]:

$$\frac{\partial}{\partial t}(\rho_a \phi) + \frac{\partial}{\partial x}(\rho_a \phi u) = 0 \tag{1}$$

$$\phi u = -\frac{k}{\mu}\frac{\partial p}{\partial x} \tag{2}$$

where $p$ is the pore pressure, $t$ is time, $k$ is the mixture permeability, $\mu$ is the fluid dynamic viscosity $\phi$ is the bed porosity, $x$ is the length coordinate, $u$ is the interstitial airflow velocity, and $\rho_a$ is the fluid density. Inertia can be neglected because of low Reynolds numbers, $Re = \rho_a\, u\, l/\mu$, where $l$ is a characteristic length scale of the flow. In our experiments, $u$ has maximum values of $\sim$10 mm/s, $\rho_a$ = 1.2 kg/m$^3$ and $\mu = 1.8 \times 10^{-5}$ Pa s (typical values of $\rho_a$ and $\mu$ for air at ambient temperature). The characteristic length, $l$, scales with pore sizes that are about equal to the particle diameter. Thus, $l \sim 60$ $\mu$m. With these considerations, Reynolds numbers $Re < 0.1$, justifying the assumption of negligible inertia. Coupling equations (1) and (2), the 1-D pore pressure equation can be expressed as [*Yilmaz et al.*, 1994; *Liang et al.*, 2001]:

$$\frac{\partial p}{\partial t} = D\frac{\partial^2 p}{\partial x^2} + D(\gamma + c_f)\left(\frac{\partial p}{\partial x}\right)^2 \tag{3}$$

where

$$D = \frac{k}{\mu\phi(c_\phi + c_f)} \tag{4}$$

$$c_\phi = \frac{1}{\phi}\frac{\partial \phi}{\partial p};\quad c_f = \frac{1}{\rho_a}\frac{\partial \rho_a}{\partial p};\quad \gamma = \frac{1}{k}\frac{\partial k}{\partial p}. \tag{5}$$

[12] $D$ corresponds to the pore pressure diffusion coefficient. The term $c_\phi$ is the so-called porosity compressibility, $c_f$ is the fluid compressibility, and $\gamma$ is known as the permeability compliance since it describes the variation of permeability with pore pressure [*Yilmaz et al.*, 1994]. The Darcy equation used for the derivation of equations (3)–(5) neglect particles velocity, and can be used for the analysis of quasi-static consolidation [*Major*, 2000]. Although this assumption appears reasonable for cases such as that investigated in the present study on the consolidation of moderately expanded mixtures, the above equations fail to predict pore pressure variations when significant grain rearrangement occurs [cf. *Iverson and LaHusen*, 1989; *Goren et al.*, 2010, 2011]. Compared with other proposed formulations [see *Goren et al.*, 2010], our model (equations (3)–(5)) appears to be adequate for studying pore pressure dynamics for a prescribed initial pore pressure (generated by means of fluidization or rapid initial particle settling) when relative particle motion is negligible (quasi-static consolidation).

[13] If volume changes of the mixture are negligible, $\phi$ remain constant so that $c_\phi \sim 0$. With this assumption, a characteristic pore pressure diffusion coefficient can be defined as $Do = k_o/(\mu\, \phi_o\, c_{fR})$, where the subscript $o$ indicates reference values of the mixture in the non-expanded and non-aerated (i.e., no air flux) state, and $c_{fR}$ denotes a reference value for the fluid (air or water) compressibility.

[14] In the following analysis, dimensionless variables are introduced,

$$p^* = p/P_L,\ x^* = x/H,\ t^* = t^*/\tau,\ k^* = k/k_o,\ \phi^* = \phi/\phi_o$$
$$c_f^* = c_f/c_{fR},\ c_\phi^* = c_\phi/c_{fR},\ \gamma^* = \gamma/c_{fR} \tag{6}$$

where the superscript * denotes dimensionless variables. $P_L$ is the lithostatic pressure at the bottom of the mixture given by $P_L = \rho\, g\, H$, $\rho$ and $H$ are the mixture density and height respectively, and $g$ is gravitational acceleration. The time scale for pore pressure diffusion is given by $\tau = L^2/Do$, where $L$ is a characteristic length scale along which pressure is diffused. As in our experiments the base of the tank can be considered impermeable, the characteristic length scale $L \sim H$ [*Iverson*, 1997; *Major*, 2000; *Iverson and Denlinger*, 2001]. Substituting the dimensionless variables of equation (6) into the pore pressure diffusion equations (equations (3)–(5)), a dimensionless form of the system of equations describing pore pressure evolution is then obtained:

$$\frac{\partial p^*}{\partial t^*} = D^*\frac{\partial^2 p^*}{\partial x^{*2}} + D^*(\gamma^* + c_f^*)c_{fR}P_L\left(\frac{\partial p^*}{\partial x^*}\right)^2 \tag{7}$$

$$D^* = \frac{D}{Do} = \frac{k^*}{\phi^*(c_\phi^* + c_f^*)} \tag{8}$$

where $D^*$ represents a dimensionless diffusion coefficient. As stated by *Yilmaz et al.* [1994], it is known that the (dimensional) coefficients $c_\phi$ and $\gamma$ are functions of $p$. To assess the relative impact of these parameters in highly confined porous media, they assumed $c_\phi$ and $\gamma$ to be pressure invariant. Here we relax such a hypothesis by assuming that the dimensionless quantities $c_\phi^*$ and $\gamma^*$ are proportional to $p^*$:

$$c_\phi^* = \alpha p^* \tag{9}$$

and

$$\gamma^* = \delta p^* \tag{10}$$

where $\alpha$ and $\delta$ are unknown constants. As it will be shown hereafter, this assumption is validated by agreement between the model and the experimental data. Substituting these relationships in the definitions of $c_\phi$ and $\gamma$ in equation (5) (using the dimensionless parameters defined in equation (6)), and integrating between the limits [0, $p^*$],

[1, $\phi$*] and [1, $k$*], the dimensionless porosity and permeability can be expressed as

$$\phi^* = \exp\left(\frac{\alpha c_{fR} P_L}{2} p^{*2}\right) \tag{11}$$

$$k^* = \exp\left(\frac{\delta c_{fR} P_L}{2} p^{*2}\right). \tag{12}$$

[15] Replacing equations (11) and (12) in equations (7) and (8) leads to

$$\frac{\partial p^*}{\partial t^*} = D^* \frac{\partial^2 p^*}{\partial x^{*2}} + D^* \left(\delta p^* + c_f^*\right) c_{fR} P_L \left(\frac{\partial p^*}{\partial x^*}\right)^2 \tag{13}$$

$$D^* = \frac{1}{\left(\alpha p^* + c_f^*\right)} \exp\left((\delta - \alpha)\frac{c_{fR} P_L}{2} p^{*2}\right). \tag{14}$$

[16] Solutions of pore pressure evolution from equations (13) and (14) depend on the value of $c_{fR}\ P_L$, which is a dimensionless parameter that compares the reference fluid compressibility with the lithostatic pore pressure. Thus, highly compressible fluids as well as thick mixtures are characterized by high values of $c_{fR}\ P_L$. In contrast, for low fluid compressibility and/or shallow mixtures, it is obvious from equation (13) that if $c_{fR} P_L \ll 1$ the quadratic term on the right hand side becomes negligible, and in equation (14) the exponential tends toward 1, thus rendering the pore pressure time variation independent of $\delta$. Hence, equations (13) and (14) can be reduced to a nonlinear diffusion equation independent of both $\delta$ and $c_{fR} P_L$,

$$\frac{\partial p^*}{\partial t^*} = D^* \frac{\partial^2 p^*}{\partial x^{*2}} \tag{15}$$

$$D^* = \frac{1}{\left(\alpha p^* + c_f^*\right)}. \tag{16}$$

[17] Low values of $c_{fR}\ P_L$ can be found in many granular mixtures, making the above simplifications relevant for the analysis. Water and air have a compressibility of $\sim 5 \times 10^{-10}$ Pa$^{-1}$ and $\sim 10^{-5}$ Pa$^{-1}$, respectively. Heights of $\sim$0.1 to $\sim$20 m are representative of many experimental and geophysical flows, for both wet and dry mixtures [*Iverson*, 1997; *Iverson and Denlinger*, 2001; *Freundt et al.*, 2000]. Considering mixture densities in the range 500–2500 kg/m$^3$ for both air- and water-solid mixtures, $P_L$ ranges from $\sim 10^2$ to $\sim 10^6$ Pa. With these limits, $c_{fR}\ P_L$ takes values of $\sim 10^{-8}$ to $\sim 10^{-4}$ for water-solid mixtures and of $10^{-3}$ to 10 for air-solid mixtures. Thus, equations (15) and (16) might be applicable for most cases of debris flows (water-solid mixtures) as well as very thin air-solid mixtures. For the experiments reported here, the mixture density is $\sim$1400 kg/m$^3$ and height is always lower than 0.5 m, so that $c_{fR}\ P_L < 0.07$. Hence, the assumption $c_{fR}\ P_L \ll 1$ may be suitable for our experiments. As it will be shown hereafter, the nonlinear pore pressure diffusion model described by equations (15) and (16) approximates well our experimental data, and so $c_{fR}\ P_L \ll 1$ will be considered in the following analysis.

[18] If pore volume changes are negligible (i.e., $c_\phi^* \sim 0$) and the fluid can be considered incompressible (i.e., $c_f^* \sim 1$), as expected for water-solid mixtures, the dimensionless pore pressure diffusion coefficient, $D$*, is approximately 1. Under these conditions, equation (15) reduces to a linear diffusion equation (equation (17)), as proposed for pore pressure diffusion in debris-flows modeling [*Iverson and Denlinger*, 2001] and for consolidating debris-flow deposits [*Major*, 2000]:

$$\frac{\partial p^*}{\partial t^*} = \frac{\partial^2 p^*}{\partial x^{*2}}. \tag{17}$$

[19] An initial condition (IC) and two boundary conditions (BC) are required to solve equation (15). The initial condition corresponds to a linear pore pressure profile, ranging from the initial dimensionless pore pressure value $\beta_o = p_{bed}/P_L$ at the base of the tank (where $p_{bed}$ is the initial pore pressure at the base of the tank), to 0 at the free surface of the mixture. Boundary conditions are given for zero pore pressure at the top and zero pore pressure flux at the base. Because a pore pressure flux in the experiments persists for a short time while the valve is turned off, an exponential decay is used to model the valve closing. Initial and boundary conditions are thus expressed as:

$$IC: \quad p^*(x^*, 0) = \beta_o (1 - x^*) \tag{18}$$

$$BC; \quad p^*(1, t^*) = 0 \qquad \frac{\partial p^*(0, t^*)}{dx} = -\beta_o \exp(-\lambda t^*) \tag{19}$$

where $\lambda = \tau/tc$, $\tau = H^2/Do$ is the vertical pore pressure diffusion time scale, and $tc$ corresponds to the characteristic closing time of the solenoid valve, $\sim$0.01 s.

[20] The dimensionless pore pressure equations (15) and (16), satisfying the specified initial and boundary conditions, were solved numerically using a finite-volume scheme with 101 nodes and a dimensionless time spacing $\Delta t^* = 0.01$ [*Patankar*, 1980; *Versteg and Malalasekera*, 1995]. The analytical solution of *Carslaw and Jaeger* [1959, pp. 97, equations 14–15] was used as a benchmark to validate our numerical model for the case of linear diffusion (i. e. $c_f^* = 1$ and $c_\phi^* = 0$).

## 4. Experimental and Numerical Studies

### 4.1. Pore Pressure Diffusion Coefficient

[21] The vertical air flux at the bottom of the tank imposed a pore fluid pressure, which determined the degree of fluidization, $\beta o$. Onset of bed expansion was observed over a narrow range of critical fluidization values ranging from $\beta o_c \sim 0.8$ for a column height of $H = 5$ cm to $\beta o_c \sim 0.9$ for column heights in the range 10–25 cm (Figure 2). Channeling and heterogeneities were observed in beds at $H = 5$ cm, which caused early onset of bed expansion [*Gilbertson et al.*, 2008]. The values of 80–90% of complete fluidization corresponding to onset of expansion agree with the findings of *Gilbertson et al.* [2008] for bed depths of 5–30 cm. Once the value of $\beta o$ surpassed $\beta o_c$, expansion of the bed increased and reached a maximum value of $\sim$8–10% at $\beta o \sim 1$ (Figure 2). The maximum degree of fluidization was

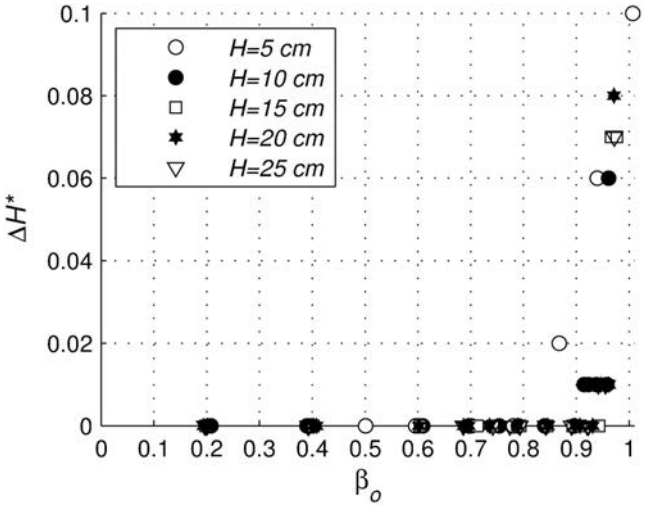



**Figure 2.** Bed expansion as a function of the initial fluidization rate, $\beta o$, for different initial bed heights ($H$). $\Delta H^* = (He - H)/H$, where $H$ is the initial (non-expanded) height and $He$ is the expanded bed height. Bed expansion occurs when $\beta o > \beta o_c$, (with $\beta o_c \sim 0.8$ for $H = 5$ cm and $\beta o_c \sim 0.9$ for $H \geq 10$ cm).

obtained in the bubbling state, whereas complete fluidization ($\beta o = 1$) was difficult to achieve.

[22] In our experiments, $c_{fR}$ $P_L$ could be neglected. Furthermore, the air compressibility may be estimated as $c_f = 1/P_{abs}$, where $P_{abs}$ is the absolute pressure. The absolute pressure corresponds to $P_{abs} = P_{atm} + p$, where $P_{atm}$ is the atmospheric pressure ($P_{atm} \sim 10^5$ Pa) and $p$ is the pore fluid pressure in excess to $P_{atm}$. As $p$ scales with $P_L$, the reference pore fluid compressibility may be estimated as $c_{fR} = 1/(P_{atm} + P_L)$. If $P_L \ll P_{atm}$, $c_{fR} \sim 1/P_{atm}$. On the contrary, if $P_L \gg P_{atm}$, $c_{fR} \sim 1/P_L$. In our experiments, $P_L$ had maximum values of ~5000 Pa, that is to say, $p$ and $P_L$ are at least two orders of magnitude smaller than $P_{atm}$, and thus $c_{fR} \sim 1/P_{atm}$. Similarly, $P_{abs} \sim P_{atm}$ whence $c_f \sim 1/P_{atm} \sim 10^{-5}$ Pa$^{-1}$, which means that the dimensionless pore fluid compressibility $c_f^* = c_f\, c_{fR}^{-1} \sim 1$. Therefore, in our experiments, the pore fluid could be considered incompressible. In addition, for $\beta o < \beta o_c$ pore volume changes were negligible, making $c_\phi^* = 0$. Thus, in the non-expanded state, ($\beta o < \beta o_c$) the simple linear diffusion equation (equation (17)) could be used to describe pore pressure diffusion. Although equation (17) seems not to be adequate for solving the pore pressure diffusion in initially expanded mixtures ($\beta o > \beta o_c$) as $c_\phi^* > 0$, and as we do not know how much our experiments deviate from the linear case, we assumed as a first approximation that the linear diffusion equation also applied for this narrow range of $\beta o$ values. Note that *Major* [2000] found experimentally that the simple linear diffusion model satisfactorily described pore pressure diffusion in consolidating (with small initial expansion <~10%) non-cohesive debris-flows deposits. Our estimates of $Do$ were obtained by fitting the linear numerical solution of the pore fluid pressure to the experimental measurements at the base of the tank, following the procedure used by *Major* [2000]. The chosen $Do$ value was the one that minimized the root mean square (rms) differences between the experimental data and the numerical results. Examples of this procedure for different $\beta o$ values are shown in Figure 3. Results show that the

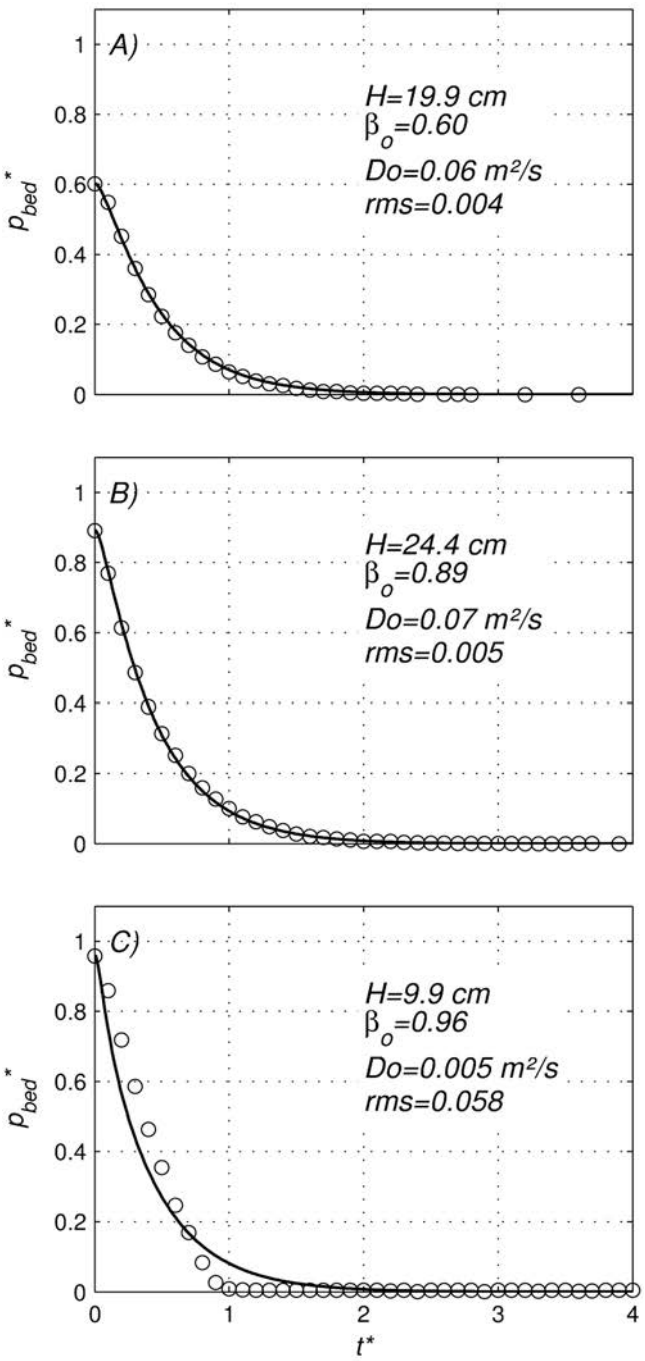



**Figure 3.** Experimental data (circles) and theoretical model (line) for the time variation of pore pressure at the base of the granular column for (a) $\beta o < \beta o_c$, (b) $\beta o$ values lower but close to $\beta o_c$ and (c) $\beta o > \beta o_c$. For column height of the order of or greater than ~10 cm, $\beta o_c \sim 0.9$. The solid line corresponds to the best fit curve with experimental data, adjusting the pore pressure diffusion coefficient, $Do$. In the figures, *rms* stands for root mean square error of the fitted curve respect to the experimental data.

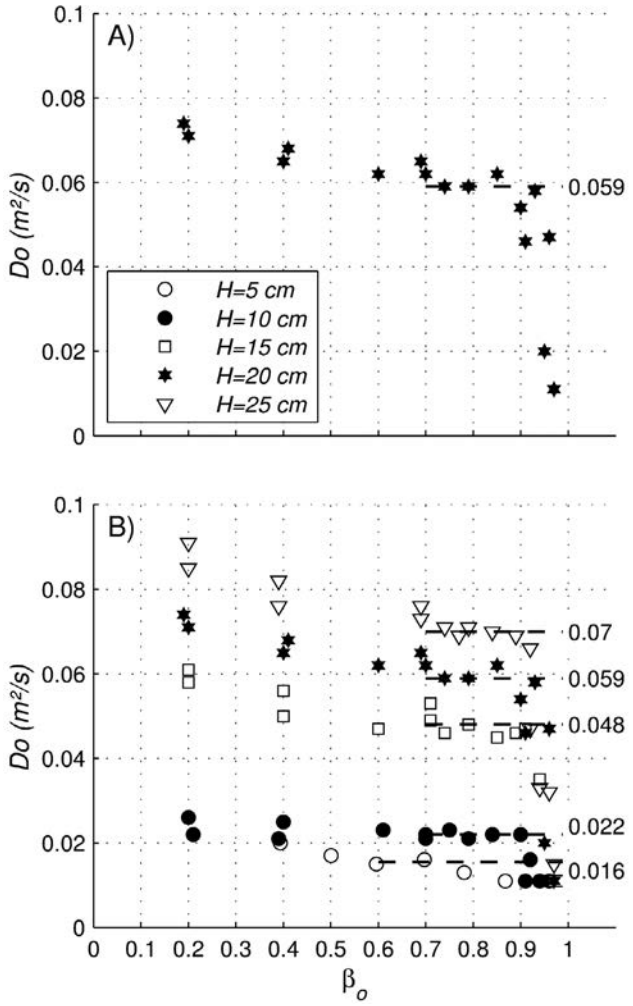



**Figure 4.** Variation of the pore pressure diffusion coefficient, *Do*, as a function of the initial degree of fluidization, $\beta o$, obtained by fitting the experimental measurements at the base of the tank with the linear diffusion model ($D^* = 1$). (a) Decrease of *Do* with $\beta o$, tending to an almost constant value of *Do* in the range $0.7 < \beta o < \beta o_c$ ($\beta o_c \sim 0.9$). When $\beta o > 0.9$, an abrupt drop in *Do* is observed. (b) The same results but for different column heights ($\beta o_c \sim 0.8$ for $H = 5$ cm and $\beta o_c \sim 0.9$ for $H > 5$ cm). Numbers on the right indicate values of *Dm*.

proposed linear model fits well the experimental data when $\beta o < \beta o_c$. For higher values of $\beta o$, the model deviates from the experimental results. In fact, Figure 3c shows that the theoretical time for the basal pore pressure diffusion is about twice that observed experimentally. This suggests that nonlinearities in the pore pressure diffusion coefficient, due to the initial expansion and continuous mixture consolidation, cannot be neglected in the analysis. In other words, $D^*$ should not be considered equal to 1 when $\beta o > \beta o_c$.

[23] The variation of *Do* as a function of $\beta o$ is presented in Figure 4. The data show that for a given height of material, *Do* slightly decreases with $\beta o$ and tends toward a nearly constant value, *Dm*, in the range $\beta o \approx 0.7$ to $\beta o_c$. For $\beta o > \beta o_c$, when the bed is expanded, fitted values of *Do* drop abruptly, suggesting that initially fluidized expanded beds retain pore pressure for longer durations, behavior that is shown in Figure 4a for a single bed height. However, this result is not conclusive, as the linear model overestimates the time of pore pressure diffusion. Figure 4b compiles the data for different bed heights, showing that for a given $\beta o$ value, *Do* increases with bed height, which is probably related to different degrees of initial bed compaction.

[24] The value of *Dm*, the mean *Do* value obtained in the range $\beta o \approx 0.7$ to $\beta o_c$, shows a linear dependence with the bed height, having a constant slope $Uc = 0.29$ m/s (Figure 5). Thus, *Uc* appears to be a characteristic velocity for pore pressure diffusion in our experiments. In the following analysis, experiments at $H = 5$ cm are not considered because strong heterogeneities and channeling in the fluidized beds did not allow for a detailed analysis.

### 4.2. Pore Pressure-Diffusion Time Scales

[25] For high degrees of fluidization before bed expansion (i.e., $0.7 < \beta o < \beta o_c$, $\beta o_c \sim 0.9$), *Do* tends to an almost constant value, *Dm*. The latter coefficient results to be a characteristic value for pore pressure diffusion in the expanded state. Thus, in the narrow range of fluidization degrees between $\beta o_c < \beta o < 1$, the pore pressure diffusion coefficient could be estimated as $D = Dm\, D^*$, where *Dm* accounts for linear diffusion while $D^*$ accounts for nonlinearities due to mixture compaction during the defluidization process. In other words, the pore pressure diffusion coefficient at high degrees of fluidization in expanded beds scales with *Dm*. To account for the importance of nonlinear effects due to the pressure diffusion process in expanded beds, the time for pore pressure diffusion obtained from the experiments is compared to that obtained by assuming a linear diffusion model, using *Dm* as a characteristic value when $\beta o_c < \beta o < 1$.

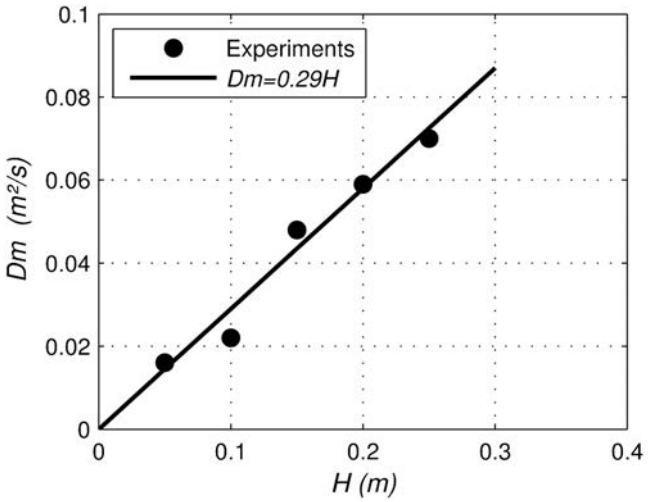



**Figure 5.** Linear dependence of *Dm*, the mean linear diffusion coefficient in the range $0.7 < \beta o < \beta o_c$ ($\beta o_c \sim 0.8$ for $H = 5$ cm and $\beta o_c \sim 0.9$ for $H > 5$ cm) in terms of the initial column height, *H*.

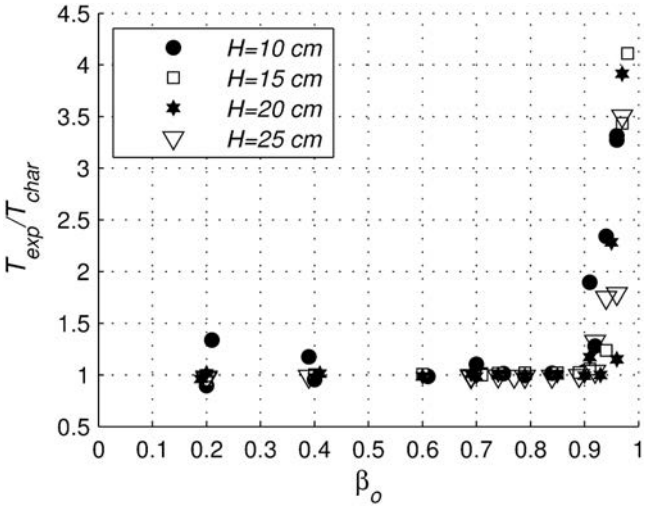



**Figure 6.** Ratio of characteristic diffusion time scales, $T_{\exp}/T_{char}$, where $T_{\exp}$ represents a characteristic dimensionless diffusion time scale estimated by means of the measured basal pore fluid pressure evolution and $T_{char}$ corresponds to a characteristic dimensionless diffusion time scale based in the linear solution for the pore fluid pressure equation. The experimental pore pressure diffusion time scale becomes larger than the theoretical linear diffusion time scale at $\beta o > \sim \beta o_c$. Values greater than 1 for $\beta o \sim 0.2$ and $\beta o \sim 0.4$ and $H = 10$ cm are attributed to errors in the experimental procedure.

[26] For a given initial fluidization degree, $\beta o$, a theoretical characteristic dimensionless diffusion time scale is defined as:

$$T_{char} = \frac{1}{\beta_0} \int p^*_{lin} dt^* \tag{20}$$

where $p^*_{lin}$ is the dimensionless pore pressure at the base of the tank obtained from the linear pore pressure equation (equation (17)). Similarly, an experimental dimensionless diffusion time scale, $T_{\exp}$, based on the measured dimensionless pressure at the base of the tank ($p^*_{measured}$) is defined as:

$$T_{\exp} = \frac{1}{\beta_0} \int p^*_{measured}\, dt^*. \tag{21}$$

[27] For the purposes of estimating $T_{\exp}$, $p^*_{measured}$ was made dimensionless using the corresponding value of $P_L$, and the dimensionless time, $t^*$, was obtained with the time scale $\tau = H^2/D_i$, where $D_i = Do$ for $\beta o < \beta o_c$ ($\beta o_c \sim 0.9$), and $D_i = Dm$ for $\beta o > \beta o_c$.

[28] Figure 6 shows the dependence of $T_{\exp}/T_{char}$ on $\beta o$. $T_{\exp}/T_{char} \sim 1$ for $\beta o < \beta o_c$, as expected because $D^* = 1$. In contrast, the time ratio increases substantially as $\beta o \sim 1$, demonstrating that bed expansion retards pore pressure diffusion by a factor of about 4 compared to the linear diffusion case. This result may seem contradictorily as the pore pressure diffusion timescale would be expected to decrease in the case of an initial bed expansion due to the increase in permeability. However, as shown by equations (4) and (8), although the pore pressure diffusion coefficient is proportional to the mixture permeability, it is inversely proportional to the mixture porosity that increases when the bed expands [*Iverson* 1997; *Major*, 2000]. Therefore, if changes in porosity outweigh changes in permeability, as porosity increases, the pore pressure diffusion should decrease, and the diffusion time scale should increase.

### 4.3. Pore Pressure Modeling of Initially Expanded Columns

[29] Porosity changes appear to be a key factor influencing pore pressure diffusion when mixtures are initially expanded. Thus, equations (15) and (16) appear more suitable for computing pore pressure diffusion in our experiments, assuming that $c_{fR} P_L \ll 1$. Equations (15) and (16) can be solved numerically for given values of $\alpha$ and $c^*_f$. In our experiments $c^*_f \sim 1$. The values of $\alpha$ in equation (16) were obtained by fitting numerical solutions of equations (15) and (16) to the experimental pressure data at the base of the tank, with $\alpha$ as a fitting parameter. For the fitting procedure, it was assumed that $D = Do\, D^*$ in non-expanded mixtures, and $D = Dm\, D^*$ in the case of expanded mixtures. Differences between the experimental data and numerical results were quantified using their root mean squares (rms), and minimized by choosing $\alpha$ as the value that minimizes the rms.

[30] Our results show that values of $\alpha$ are near zero for $\beta o < \beta o_c$, as linear diffusion applies for fluidization degrees below those causing bed expansion (Figure 7). In contrast, for $\beta o > \beta o_c$, $\alpha$ values increase up to $\sim$10 for near complete fluidization, showing that the linear pore pressure diffusion coefficient ($Dm$) could be reduced by about one order of magnitude in expanded beds at maximum fluidization ($p^* = 1$). This corresponds to maximum values of $c_\phi = c^*_\phi\, c_{fR} \sim 10^{-4}$ Pa$^{-1}$, which are several orders of magnitude larger than values commonly reported for pressure diffusion in confined porous media (e.g., $c_\phi \sim 0.15 \times 10^{-9}$–$15 \times 10^{-9}$ Pa$^{-1}$ [*Yilmaz et al.*, 1994; *Hummel*, 2008]) and

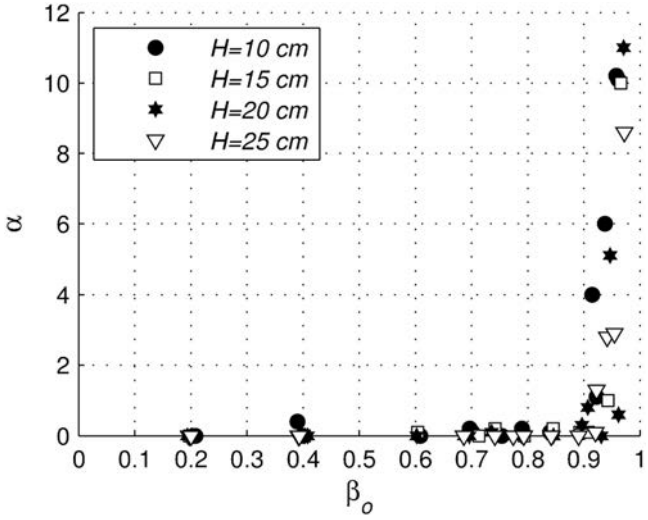



**Figure 7.** Fitted values of $\alpha$ as a function of $\beta o$ for different initial heights. For $\beta o < \beta o_c$, when the bed is not expanded and the linear diffusion model is applicable, values of $\alpha$ are equal to zero.

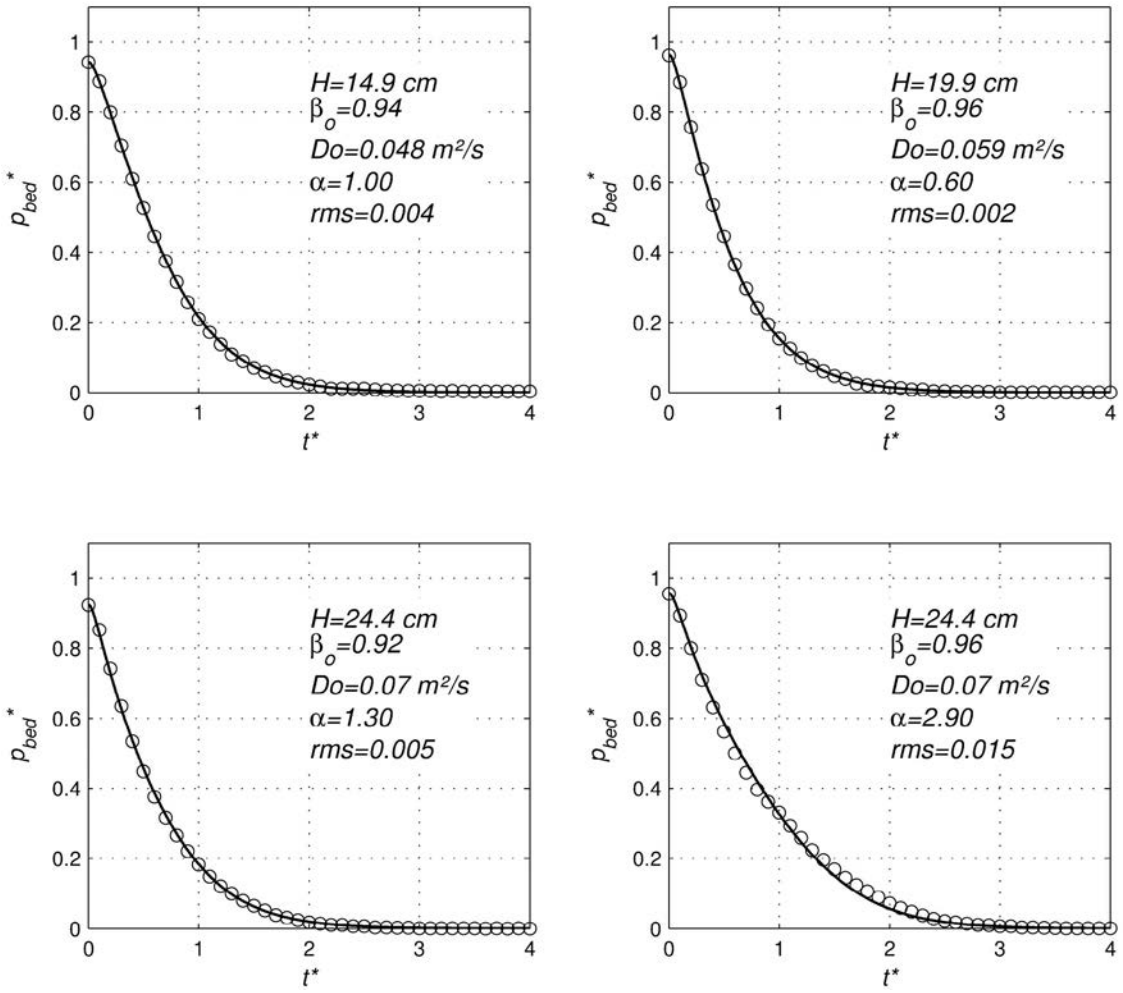



**Figure 8.** Experimental data (circles) and numerical fit (line) at the base of the tank for initially expanded mixtures ($\beta o > \beta o_c$) using equations (15) and (16). In the figures, *rms* stands for root mean square error of the fitted curve respect to the experimental data.

about 10 times greater than values reported for self-consolidating debris-flows mixture [*Major*, 2000].

[31] Taking into account the fitted values of $\alpha$, excellent agreement is achieved between the experimental and numerical results for the time needed to diffuse pore fluid pressure (Figure 8). This agreement shows that the proposed model adequately describes pore pressure evolution of initially expanded mixtures. Note that if $\alpha = 0$ in equation (15) (and because $c_f^* \sim 1$), the linear diffusion equation is recovered as $D^* = 1$. Thus, the proposed model adequately predicts pore pressure evolution in non-expanded mixtures. Our results show that when the interstitial fluid is air, assumptions that simplify the pore pressure equations, specifically $c_{fR} P_L \ll 1$ and $c_f^* = 1$, are adequate for modeling the pore fluid pressure time evolution. Such assumptions neglect pore fluid compressibility effects.

[32] An important increase in the time scale of pore pressure diffusion is observed as $\alpha$ increases. Numerical results obtained for the case of a fully fluidized mixture ($\beta o = 1$) show that for the linear diffusion case ($\alpha = 0$) pore pressure diffuses almost entirely at $t^* \sim 2$ (Figure 9). However, excess pore pressure persists until $t^* \sim 3$ when $\alpha = 5$, and until $t^* \sim 5$ when $\alpha = 10$. Therefore, changes in the porosity compressibility ($c_\phi$), resulting from column consolidation, control the diffusion of excess pore pressure in expanded granular material. Additionally, the proposed numerical model provides the time pore pressure evolution at any height within the mixture for a given value of $\alpha$.

[33] In initially expanded beds, the local pore pressure diffusion coefficient at a given time is a function of the local pore pressure, thus the pore pressure diffusion coefficient varies with both time and height (Figure 10). For given values of $\alpha > 0$, the diffusion coefficient is maximum at the top of the granular column, as $D^* = 1$, and progressively reduces toward the bottom of the column. The dimensionless diffusion coefficient $D^*$, decreases as $\alpha$ increases, reaching minimum values of the order of 0.1 at the bottom of the granular column for the maximum values of $\alpha \sim 10$. For linear diffusion ($\alpha = 1$), $D^*$ is constant and equal to 1, independently of time and height. In expanded beds, the return to a linear diffusion behavior ($D^* = 1$) is slowly and asymptotically achieved. Figure 10 shows that the time taken for $D^*$ at the bottom of the granular column to reach values of $D^* \sim 1$ is longer than that of pore pressure diffusion. For example, it takes about $t^* = 4$ and more than $t^* = 5$ to reach $D^* \sim 1$ for cases at $\alpha = 5$ and $\alpha = 10$, respectively,

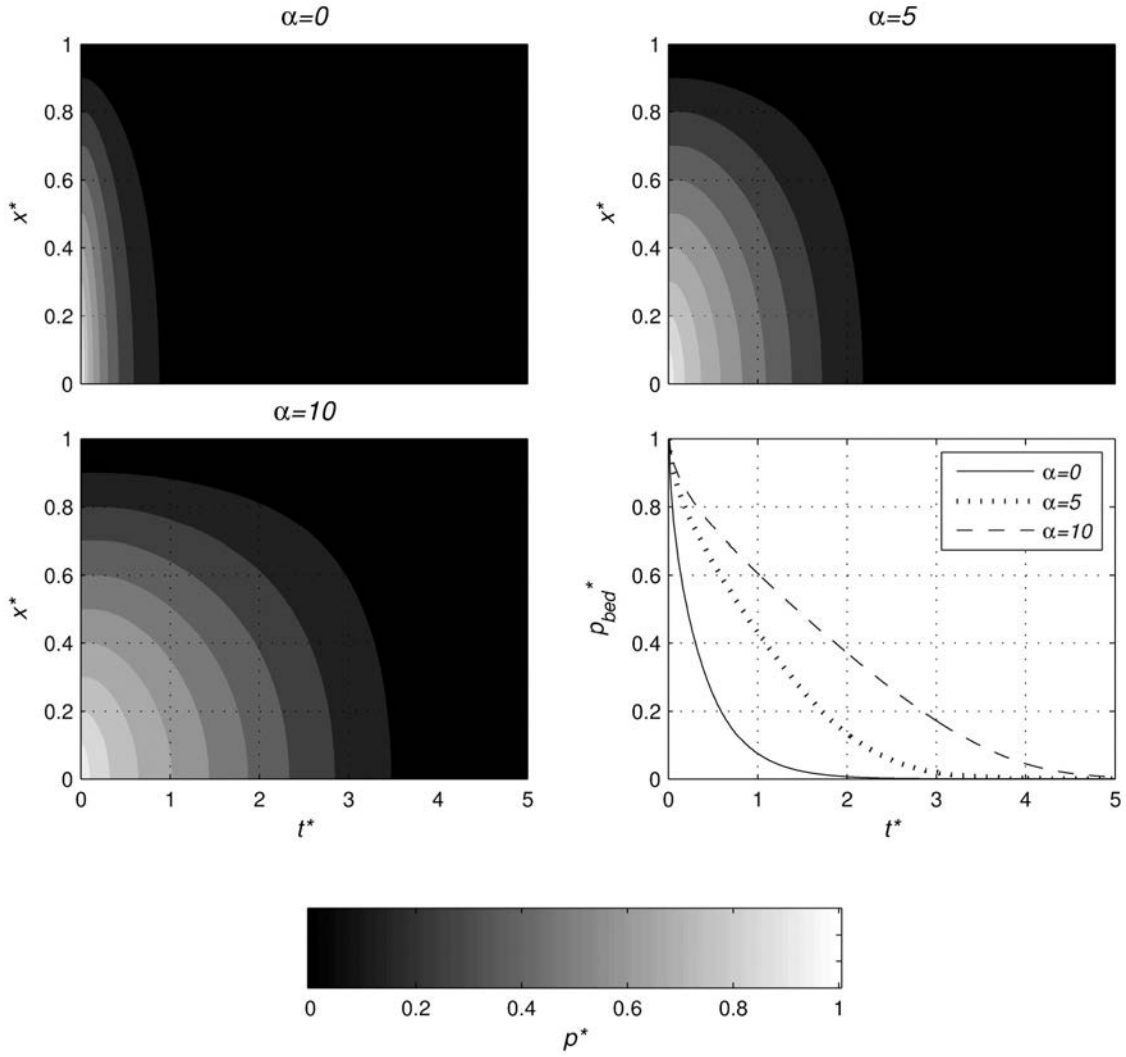



**Figure 9.** Vertical profile of the dimensionless pore pressure time evolution ($p^*$) for an initially fully fluidized granular bed and different $\alpha$ values using equations (15) and (16). Values of $\alpha$ vary in the range of 0 to 10 (Figure 7). The solutions shown for $\alpha = 0$ correspond to those of linear diffusion. The term $p^*_{bed}$ at the right bottom corner represents the dimensionless pore fluid pressure at the base of the granular column. The color bar represents values of $p^*$.

while pore pressure is almost entirely diffused at $t^* = 3$ and $t^* = 4$ for the same conditions (Figures 9 and 10).

## 5. Discussion

### 5.1. Pore Pressure Diffusion in Initially Aerated Granular Columns

[34] Pore pressure diffusion in aerated granular mixtures shows remarkably variable behavior that depends on the degree of initial bulk expansion. For non-expanded beds, pore pressure diffusion follows a simple linear diffusion model, with a constant value for the diffusion coefficient. In contrast, the pore pressure diffusion coefficient in initially expanded beds is pressure dependent, evolving as long as pore pressure diffuses within the granular mixture. As shown by equation (4), $D$ is a function of permeability ($k$), porosity ($\phi$), fluid viscosity ($\mu$), mixture compressibility ($c_\phi$) and fluid compressibility ($c_f$). In our experiments (as well as those using wet debris-flow material or shallow air-particles mixtures), fluid can be treated as uncompressible, thus $c_f$ is nearly constant. Furthermore, changes in fluid viscosity are negligible, although fine particles (dust or colloids) can increase the bulk viscosity in some geophysical mixtures [*Iverson*, 1997; *Major*, 2000]. Though permeability appears relevant for the reference pressure diffusion coefficients ($Do$, $Dm$), our numerical model shows that changes in permeability can be neglected, even when permeability varies significantly under small changes of porosity. Note that, the dependence of $D$ on $k$ and $\phi$ has been previously addressed by *Iverson* [1997] and *Major* [2000].

[35] *Major* [2000] showed that for a wide range of debris flow mixture permeabilities ($10^{-9}$ m$^2$ to $10^{-14}$ m$^2$) low pore pressure diffusivities are not solely influenced by low permeability. High mixture compressibility (or porosity compressibility) in initially dilated mixtures under low effective stress also influences pore pressure diffusion and contributes

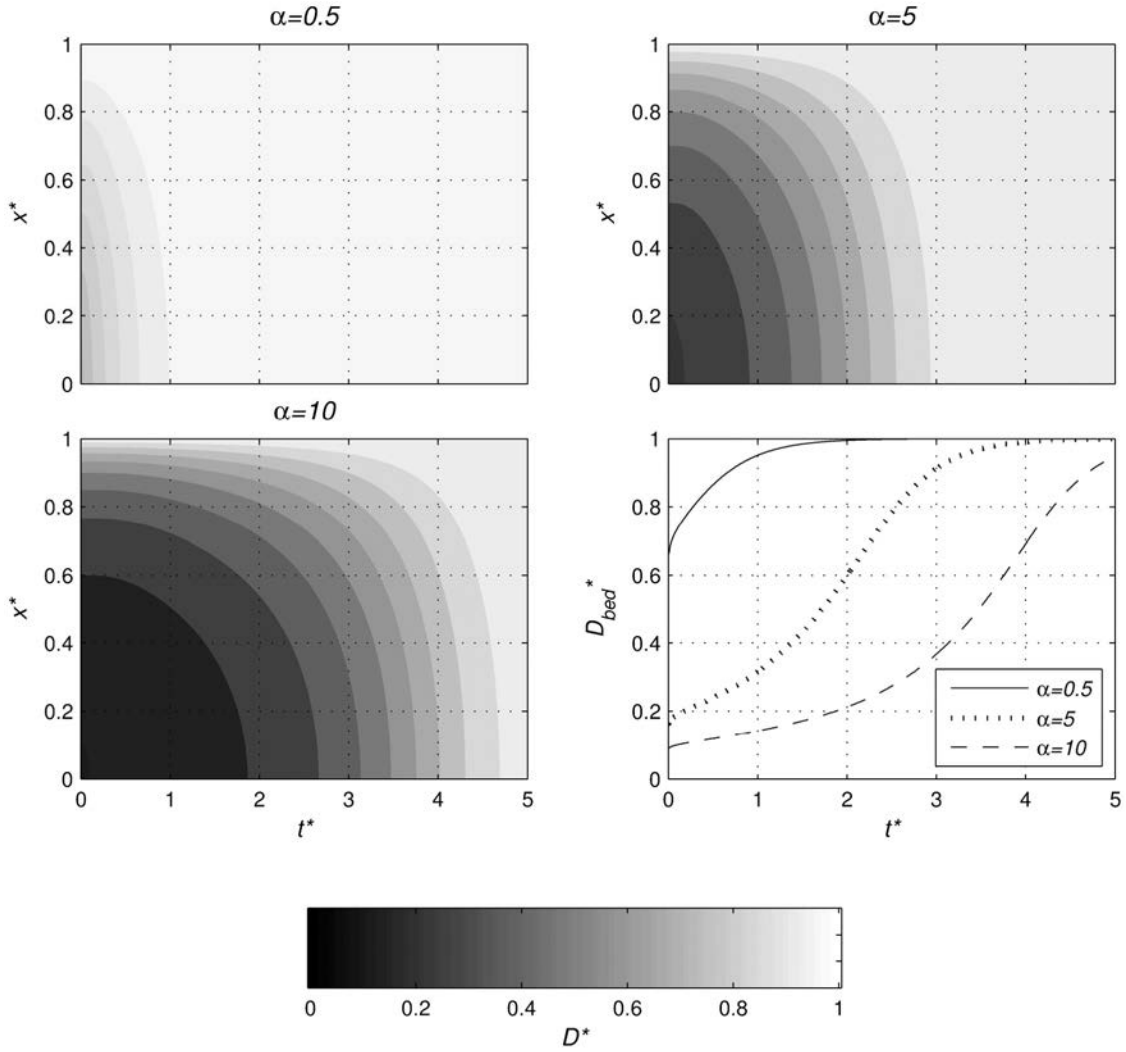



**Figure 10.** Vertical profile of the diffusion coefficient time evolution ($D^*$) for an initially fully fluidized granular bed and different $\alpha$ values using equations (15) and (16). Values of $\alpha$ vary in the range of 0.5 to 10 (Figure 7). The solution for $\alpha = 0$ (i. e. linear diffusion) is not shown, as in this case $D^*$ is constant and equal to 1. $D^*_{bed}$ at the right bottom corner represents the dimensionless fluid diffusion coefficient at the base of the granular column. The color bar represents values of $D^*$.

to low diffusivity coefficients. In some mixtures, changes in compressibility can outweigh changes in permeability [*Major*, 2000]. In our experiments, using initially expanded beds, mixture compressibility strongly affected pore pressure diffusion. As shown by equation (16), the dimensionless pore pressure diffusion coefficient, $D^*$, is a function solely of the pore compressibility ($c^*_\phi = \alpha\, p^*$). In this study $c_\phi \sim 10^{-4}$ Pa$^{-1}$, that is, one order of magnitude higher than in *Major* [2000] ($c_\phi \sim 10^{-5}$ Pa$^{-1}$). This explains why the linear model applies better to the debris-flow mixtures tested by *Major* [2000] than to our experiments. For non-expanded mixtures, where $c_\phi \approx 0$, the linear model provides good results. As shown by equations (13) and (14), permeability changes, represented by the permeability compliance ($\gamma$), are multiplied by $c_{fR}\, P_L$. Therefore, permeability changes ($\gamma$) do not contribute to the pore pressure diffusion process when fluid compressibility effects are negligible ($c_{fR}\, P_L \ll 1$), As a result, changes in porosity do not just outweigh changes in permeability, but instead changes in permeability are typically negligible when $c_{fR}\, P_L \ll 1$.

[36] The parameter $c_{fR}\, P_L$ shows that pore fluid compressibility effects are not solely a function of fluid compressibility, but are also a function of effective stress, which in our case scaled with the lithostatic pressure $P_L$. Thus, even for low compressible fluids, fluid compressibility could affect pore pressure diffusion in highly confined systems, such as deep groundwater or hydrocarbons reservoirs [*Yilmaz et al.*, 1994; *Hummel*, 2008], in which case permeability compliance could become relevant. However, this might not be applicable for most unconfined, self-consolidating mixtures such as natural granular mixtures.

### 5.2. Time Scales of the Pore Pressure Diffusion Process

[37] For estimating pore pressure diffusion time scales in our experiments, we calculate $T^*_D$, the dimensionless time required for basal pore pressure to reach 1% of the initial degree of fluidization (i.e., $p^*_o = 0.01\ \beta o$), according to the

proposed numerical model. This cutoff value was chosen arbitrarily for convenience since the diffusion model decreases asymptotically to $p^* = 0$. For calculations, $\alpha = 0$ was considered when $0 \le \beta o \le \beta o_c$. In the range $\beta o_c \le \beta o \le 1$, it was supposed that $\alpha$ varied linearly from 0 to 10. The obtained diffusion timescale has a constant value $T_D^* = 1.84$ for $0 \le \beta o \le \beta o_c$. In contrast, once the bed is expanded ($\beta o_c \le \beta o \le 1$), $T_D^*$ increases linearly up to 4.74 ($\beta o = 1$, fully fluidized mixture). Thus, a break in the tendency occurs when $\beta o > \beta o_c$ with a maximum about 2.6 times greater than the constant value of $T_D^*$ (in the range $0 < \beta o < \beta o_c$) when $\beta o = 1$. A similar break in tendency was previously reported for the run-out distance of initially aerated granular flows of almost the same particle mixtures [*Montserrat et al.*, 2007; *Roche et al.*, 2008]. The run-out distance showed a little increase between $0 < \beta o < \beta o_c$, but importantly increased to almost twice that observed for $\beta o = \beta o_c$, when $\beta o = 1$. This result suggested that the initial degree of fluidization, and related mixture expansion when $\beta o > \beta o_c$, controlled most of the flow dynamics and run-out distance. It is worth mentioning that for comparison with experiments of *Roche et al.* [2008], it is assumed that $\beta o_c$ was reached at $\sim Umf$ and complete fluidization (i.e., $\beta o = 1$) was obtained at $\sim Umb$. In complementary experiments, *Roche et al.* [2010] measured the pore pressure at the base of initially fluidized and expanded flows (cf. $\beta o = 1$). They reported that the duration of pore pressure diffusion was close to the duration of the flows and also to the duration of pressure diffusion in defluidizing static columns of similar heights. As a matter of fact our method predicts, at $\beta o = 1$ ($T_D^* \sim 5$), that the duration of pressure diffusion is close to the flow duration reported by *Roche et al.* [2010]. This supports the idea that the dynamics of initially fluidized flows are controlled by overall mixture compaction and associated pore pressure diffusion, as observed in our self-consolidating static experiments.

[38] The time scale for pressure diffusion cannot be directly extrapolated to other conditions, as it is mixture dependent. However, because $\alpha$ is related only to the pore compressibility, it should be a function of the range of dilation or compaction that can be attained for a given mixture. In case of quasi-static consolidation, $\alpha$ scales with the initial degree of expansion, so that more expanded mixtures attain larger values of $\alpha$. The nature of the interstitial fluid does not appear to affect the value of $\alpha$, but as our experiments focused on just one type of air-particle mixtures this needs further research. It is also known that the amount of initial expansion of gas-fluidized mixtures depends on the grain size distribution. In particular, the mixture expansion increases with the amount of fine particles. For instance, ash-rich pyroclastic flow materials, with particle diameters in the range $\sim 1$ $\mu$m to 250 $\mu$m, can have maximum expansions near 50% [*Druitt et al.*, 2007; *Girolami et al.*, 2008], which would result in larger values of $\alpha$ than those determined here. Furthermore, increasing the amount of fines reduces the mixture permeability by clogging connected pores and inhibiting the ease of fluid flows. Thus, the reduction in permeability due to fine particles can effectively reduce the reference pore pressure diffusion coefficient, thus increasing the time needed to diffuse the excess pore fluid pressure and even in non-expanded mixtures [*Major*, 2000; *Lorences et al.*, 2003].

### 5.3. Insights into Geophysical Granular Flow Processes

[39] In initially expanded granular mixtures, our results highlight the effects that mean mixture compaction has in retarding pore fluid pressure. Pore fluid pressure measured at the base of granular flows often reveals a complex behavior [*Iverson* 1997; *Iverson et al.*, 2010; *Roche et al.*, 2010]. Our study, however, suggests that initial material expansion (due to a certain degree of fluidization) may explain much of the bulk flow dynamics in small-scale, fine-grained, mono-disperse granular flows with low pore pressure -diffusion coefficients ($D \sim 0.01$–$0.02$ m$^2$/s). Note that these values of $D$ are in the range inferred for thin ash-rich pyroclastic flows on the basis of their material permeability [*Druitt et al.*, 2007]. For debris flows, pore pressure-diffusion coefficients range between $D \sim 10^{-7}$–$10^{-3}$ m$^2$/s [*Iverson*, 1997; *Major et al.*, 1997; *Major and Iverson*, 1999; *Major*, 2000]. Thus, in wet flows, pore pressure diffusion takes longer than in air-particle mixtures of similar size. Fine particles clearly affect the value of $D$, effectively retarding pore pressure diffusion, as shown experimentally for debris flows [*Major and Iverson*, 1999; *Major*, 2000] and pyroclastic-flow material [*Druitt et al.*, 2007]. Although our mono-disperse air-particle mixtures lack the range of grain size distribution typical of most natural geophysical flows, fine group-A-type air-particle mixtures may replicate most of the observed characteristics of pore pressure diffusion in natural flows containing large amounts of fines. Despite the reduced scale of our experiments ($H < \sim 0.5$ m) compared to natural geophysical flows, our results highlight the mechanisms retarding pore fluid-pressure diffusion. Note, however, that the size of some of the smaller flows in nature is of the same order of that of our experiments. For instance, distal deposits of pyroclastic flows are commonly a few decimeters thick [*Druitt*, 1998; *Freundt et al.*, 2000; *Wilson and Head*, 1981]. In this context, our findings should apply well to pyroclastic flows with $D$ values similar to those presented in this paper.

[40] In the present study, we assumed that pore fluid compressibility effects are negligible even when the pore fluid is air, which is a consequence of the shallow mixture heights in our experiments. This assumption is appropriate for wet debris flows (or any water-particle mixture), but may not be valid for thick gas-particles mixtures such as large pyroclastic flows and snow avalanches. Figure 11 shows values of the product $c_{fR} P_L$ for our experimental granular mixtures and natural geophysical flows. As in air particle-mixtures the fluid compressibility can be calculated as $c_{fR} = 1/(P_{atm} + P_L)$, in thick flows, where $P_L \gg P_{atm}$, the product $c_{fR} P_L$ approaches 1. For natural flows shown in Figure 11, we considered typical values of mixture densities to estimate $P_L$. Values of the product $c_{fR} P_L$ in our experiments are comparable to those of thin pyroclastic flows ($H < 1$ m). For thick pyroclastic flows ($H > 10$ m) $c_{fR} P_L \sim 1$, implying that pore fluid pressure compressibility is not negligible and that the permeability compliance ($\gamma$) has an important effect on the pore pressure diffusion process. In particular, if $c_{fR} P_L$ is non-negligible, the quadratic term on the right hand side of equation (13) may promote pore fluid-pressure generation. Furthermore, the exponential term affecting the pore pressure diffusion coefficient (equation (14)) can become non-negligible, and thus can accelerate the diffusion process.

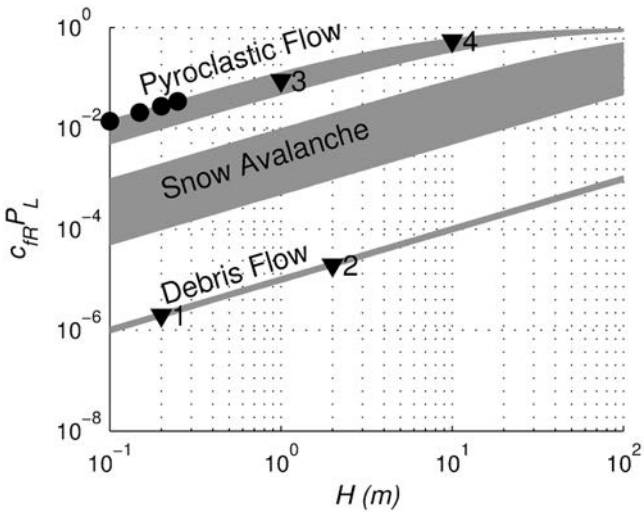



**Figure 11.** Estimates of $c_{fR}\ P_L$ for different types of geophysical granular flows and our laboratory experiments. Reference values of the pore fluid compressibility ($c_{fR}$) are assumed to be $5 \times 10^{-10}$ Pa$^{-1}$ and $10^{-5}$ Pa$^{-1}$ in the case of water-particle (debris flow) and air-particle (pyroclastic flows and snow avalanches) mixtures, respectively. Mixture densities are assumed within the range 1800–2300 kg/m$^3$ for debris flows [*Iverson*, 1997; *Iverson and Vallance*, 2001; *Hauser*, 2002], 10–1000 kg/m$^3$ for snow avalanches [*McClung and Schaerer*, 1993; *Turnbull and McElwaine*, 2007], and 500–1500 kg/m$^3$ for pyroclastic flows [*Druitt*, 1998; *Freundt et al.*, 2000]. Flow heights, $H$, are in the range 0.1–100 m. Black dots represent the values of $c_{fR}\ P_L$ in the present experiments, while black triangles correspond to estimations of $c_{fR}\ P_L$ values computed out of the granular flow data reported by *Iverson and Denlinger* [2001]: 1) experimental USGS debris flows, 2) Yake Dake, debris flow, 3) small-volume pumice pyroclastic flow deposits of Mount St. Helens and 4) Elm rock Avalanche.

Detailed effects of the permeability compliance on pore pressure diffusion are beyond the scope of this work.

## 6. Conclusions

[41] Pore pressure diffusion in initially aerated, air-particle mixtures was investigated through experiments and numerical modeling. Experiments recorded the decay of the pore fluid pressure at the base of an initially aerated granular column. Pressure data were compared with a 1D numerical model obtained by coupling the continuity equation with the Darcy equation for estimating air velocity and assuming negligible particle relative motion (quasi-static consolidation). A dimensional analysis shows that fluid compressibility and changes in permeability can be neglected for modeling our experiments. Thus, the proposed pore pressure equation reduces to a simpler diffusion equation with a variable diffusion coefficient, $D$. When pore volume changes are negligible (no expansion or contraction), $D$ is constant and pore pressure can be modeled using a simple linear diffusion equation. This approach has been extensively used in previous works for the analysis of quasi-static soil consolidation and it provided good results for predicting pore fluid pressure evolution in our experimental mixtures that were not initially expanded. On the other hand, when our mixtures were initially expanded, nonlinear effects due to mixture consolidation became important during the pore pressure diffusion process.

[42] Porosity compressibility ($c_\phi$) appears to be a key parameter for estimating the value of the nonlinear diffusion coefficient. Large values of $c_\phi$ reduce the reference pore pressure-diffusion coefficient ($D \sim 1/c_\phi$) and retard pore pressure diffusion in granular mixtures. Thus, highly dilative (and then contractive) mixtures, with associated large values of $c_\phi$, can maintain excess pore fluid pressure for longer durations compared to less compressible mixtures. Pore pressure diffusion during mixture compaction in our experimental static columns, occurred over time scales comparable to durations of experimental initially fluidized granular flows of similar heights [*Roche et al.*, 2008, 2010], suggesting that our model for static configurations can be applied to flowing mixtures. This is being tested with new experimental results. Although permeability is an important variable that controls the reference pore pressure diffusion coefficient, changes in permeability were negligible in our experiments because they were outweigh by changes in porosity and because pore fluid compressibility effects were negligible. Our results highlight that porosity compressibility can effectively retard pore pressure diffusion in initially expanded dry-granular mixtures and depends chiefly on changes in pore volume size, so that particle-size distribution is important in controlling pressure diffusion. However, because our experiments focused on mono-disperse mixtures, this conclusion deserves further research.

## Notation

$\alpha$ proportional coefficient for estimating $c_\phi$*, dimensionless.
$\beta_o$ initial degree of fluidization ($p_o/P_L$), dimensionless
$\beta o_c$ initial degree of fluidization at the onset of bed expansion, dimensionless.
$\delta$ proportional coefficient for estimating $\gamma$*, dimensionless
$\Delta H$* dimensionless initial bed expansion.
$\Delta t$* dimensionless time spacing for the numerical solution.
$\phi$ mixture porosity, dimensionless.
$\phi$* rescaled mixture porosity, dimensionless.
$\gamma$ permeability compliance, Pa$^{-1}$.
$\gamma$* dimensionless permeability compliance.
$\lambda$ dimensionless time scale associated to the closing of the solenoid valve.
$\mu$ interstitial fluid dynamic viscosity, Pa s.
$\rho$ mixture density, Kg/m$^3$.
$\rho_a$ interstitial fluid density, Kg/m$^3$.
$\tau$ pore pressure diffusion time scale, s.
$c_\phi$ porosity compressibility, Pa$^{-1}$.
$c_\phi^*$ dimensionless porosity compressibility.
$c_f$ fluid compressibility, Pa$^{-1}$.
$c_f^*$ dimensionless fluid compressibility.
$c_{fR}$ reference value for the fluid (air or water) compressibility, Pa$^{-1}$.
$D$ pore pressure diffusion coefficient, m$^2$/s.
$D$* dimensionless pore pressure diffusion coefficient.

$D^*_{bed}$ dimensionless pore pressure diffusion coefficient at the base of the granular column.

$Dm$ characteristic pore pressure diffusion for initially expanded beds ($\beta o > \beta o_c$), $m^2/s$

$Do$ characteristic pore pressure diffusion coefficient (in the non-expanded, non-aerated state), $m^2/s$.

$g$ gravitational acceleration, $m/s^2$.

$H$ mixture height, m.

$He$ expanded bed height, m.

$k$ mixture permeability, $m^2$.

$k^*$ dimensionless mixture permeability.

$L$ characteristic length scale for pore pressure diffusion, m.

$p$ pore pressure, Pa.

$p^*$ dimensionless pore pressure.

$p_{bed}$ pore pressure at the base of the granular column, Pa.

$p^*_{bed}$ dimensionless pore pressure at the base of the granular column.

$p^*_{lin}$ dimensionless pore pressure at the base of the tank obtained from the linear pore pressure equation

$p^*_{measured}$ experimental dimensionless diffusion time scale, based on the measured pressure.

$P_{abs}$ absolute pressure, Pa.

$P_{atm}$ atmospheric pressure, Pa.

$P_L$ lithostatic pressure (particles weight divided by the cross-sectional area of the container), Pa.

$t$ time, s.

$t^*$ dimensionless time.

$tc$ characteristic closing time of the solenoid valve, s.

$T_{char}$ characteristic dimensionless diffusion time scale based in the linear solution for the pore fluid pressure.

$T^*_D$ dimensionless time elapsed for the basal pore pressure to reach 1% of the initial degree of fluidization.

$T_{\exp}$ characteristic dimensionless diffusion time scale estimated by means of the measured basal pore fluid pressure evolution.

$u$ interstitial air velocity, m/s.

$Uc$ characteristic scale velocity for pore pressure, m/s

$Umb$ minimum bubbling velocity, m/s.

$Umf$ minimum fluidization velocity (or velocity at the onset of bed expansion), m/s.

$x$ vertical length coordinate, m.

$x^*$ dimensionless vertical length coordinate.

[43] **Acknowledgment.** The first author acknowledges the financial support from project Mecesup UCH 310, in the form of a PhD fellowship and Departamento de Postgrado y Postítulo de la Vicerrectoría de Asuntos Académicos, Universidad de Chile, as a foreign residence fellowship. This work was supported by ECOS-CONICYT Projects C06U01 and C11U01, Institut de Recherche pour le Développement (IRD, France), ANR (France), Departamento de Ingeniería Civil, Universidad de Chile and Advanced Mining Technology Center (AMTC). The authors acknowledge the valuable comments made by the Associate Editor during the review process.

## References

Aharonov, E., and D. Sparks (1999), Rigidity phase transition in granular packings, *Phys. Rev. E*, *60*(6), 6890–6896, doi:10.1103/PhysRevE.60.6890.

Ancey, C. (2007), Plasticity and geophysical flows: A review, *J. Non-Newtonian Fluid Mech.*, *142*, 4–35, doi:10.1016/j.jnnfm.2006.05.005.

Ancey, C., and P. Evesque (2000), Frictional-collisional regime for granular suspension flows down an inclined channel, *Phys. Rev. E*, *62*(6), 8349–8360, doi:10.1103/PhysRevE.62.8349.

Armanini, A., H. Capart, L. Fraccarollo, and M. Larcher (2005), Rheological stratification in experimental free-surface flows of granular-liquid mixtures, *J. Fluid Mech.*, *532*, 269–319, doi:10.1017/S0022112005004283.

Armanini, A., L. Fraccarollo, and M. Larcher (2008), Liquid-granular channel flow dynamics, *Powder Technol.*, *182*, 218–227, doi:10.1016/j.powtec.2007.08.012.

Azanza, E., F. Chevoir, and P. Moucheront (1999), Experimental study of collisional granular flows down an inclined plane, *J. Fluid Mech.*, *400*, 199–227, doi:10.1017/S0022112099006461.

Bagnold, R. A. (1954), Experiments on a gravity-free dispersion of large solid spheres in a Newtonian fluid under shear, *Proc. R. Soc. London, Ser. A*, *225*, 49–63, doi:10.1098/rspa.1954.0186.

Bareschino, P., A. Marzocchella, P. Salatino, L. Lirer, and P. Petrosino (2008), Self-fluidization of subaerial rapid granular flows, *Powder Technol.*, *182*, 323–333, doi:10.1016/j.powtec.2007.12.010.

Campbell, C. S. (1990), Rapid granular flows, *Annu. Rev. Fluid Mech.*, *22*, 57–90, doi:10.1146/annurev.fl.22.010190.000421.

Carslaw, H. S., and J. C. Jaeger (1959), *Conduction of Heat in Solids*, 2nd ed., Oxford Univ. Press, New York.

Davidson, J. F., and D. Harrison (1971), *Fluidization*, Academic Press, New York.

Denlinger, R. P., and R. M. Iverson (2001), Flow of variably fluidized granular masses across three-dimensional terrain: 2. Numerical predictions and experimental tests, *J. Geophys. Res.*, *106*, 553–566, doi:10.1029/2000JB900330.

Druitt, T. H. (1998), Pyroclastic density currents, *Geol. Soc. Spec. Publ.*, *145*, 145–182.

Druitt, T. H., G. Avard, G. Bruni, P. Lettieri, and F. Maez (2007), Gas retention in fine-grained pyroclastic flow materials at high temperatures, *Bull. Volcanol.*, *69*, 881–901, doi:10.1007/s00445-007-0116-7.

Freundt, A., S. Carey, and C. J. N. Wilson (2000), Ignimbrites and block-and-ash flow deposits, in *Encyclopedia of Volcanoes*, edited by H. Sigurdsson et al., pp. 581–600, Academic, New York.

Geldart, D. (1973), Types of gas fluidization, *Powder Technol.*, *7*, 285–292, doi:10.1016/0032-5910(73)80037-3.

Geldart, D., and A. C. Y. Wong (1985), Fluidization of powders showing degrees of cohesiveness—II. Experiments on rates of deaeration, *Chem. Eng. Sci.*, *40*, 653–661, doi:10.1016/0009-2509(85)80011-7.

George, D. L., and R. M. Iverson (2011), A two-phase debris-flow model that includes coupled evolution of volume fractions, granular dilatancy, and pore-fluid pressure, in *Debris-Flow Hazard Mitigation: Mechanics, Prediction and Assessment*, pp. 415–424, Am. Soc. Of Civ. Eng., New York.

Gibilaro, L. (2001), *Fluidization-Dynamics*, Butterworth-Heinemann, Boston, Mass.

Gilbertson, M. A., D. E. Jessop, and A. J. Hogg (2008), The effects of gas flow on granular currents, *Philos. Trans. R. Soc. A*, *366*, 2191–2203, doi:10.1098/rsta.2007.0021.

Girolami, L., T. H. Druitt, O. Roche, and Z. Khrabrykh (2008), Propagation and hindered settling of laboratory ash flows, *J. Geophys. Res.*, *113*, B02202, doi:10.1029/2007JB005074.

Goldhirsch, I. (2003), Rapid granular flows, *Annu. Rev. Fluid Mech.*, *35*, 267–293, doi:10.1146/annurev.fluid.35.101101.161114.

Goren, L., E. Aharonov, D. Sparks, and R. Toussaint (2010), Pore pressure evolution in deforming granular material: A general formulation and the infinitely stiff approximation, *J. Geophys. Res.*, *115*, B09216, doi:10.1029/2009JB007191.

Goren, L., E. Aharonov, D. Sparks, and R. Toussaint (2011), The mechanical coupling of fluid-filled granular material under shear, *Pure Appl. Geophys.*, *168*, 2289–2323, doi:10.1007/s00024-011-0320-4.

Hauser, A. (2002), Rock avalanche and resulting debris flow in Estero Parraguirre and Río Colorado, Región Metropolitana, Chile, in *Catastrophic Landslides: Effects, Occurrence, and Mechanisms*, *Rev. Eng. Geol.*, vol. 15, edited by S. Evans and J. V. DeGraff, pp. 135–148, Geol. Soc. Am., Boulder, Colo.

Hummel, N. (2008), Modelling and interpretation of microseismic signatures related to nonlinear pore pressure diffusion in porous media, Diploma thesis, Geophys. Inst. Univ. Karlsruhe (TH), Karlsruhe, Germany.

Hutter, K., Y. Wang, and S. P. Pudasaini (2005), The Savage-Hutter avalanche model: How far can it be pushed? *Philos. Trans. R. Soc. A*, *363*, 1507–1528, doi:10.1098/rsta.2005.1594.

Iverson, R. M. (1997), The physics of debris flows, *Rev. Geophys.*, *35*, 245–296, doi:10.1029/97RG00426.

Iverson, R. M., and R. P. Denlinger (2001), Flow of variably fluidized granular masses across three-dimensional terrain: 1. Coulomb mixture theory, *J. Geophys. Res.*, *106*, 537–552, doi:10.1029/2000JB900329.

Iverson, R. M., and R. G. LaHusen (1989), Dynamic pore-pressure fluctuations in rapidly shearing granular-materials, *Science*, *246*, 796–799, doi:10.1126/science.246.4931.796.

Iverson, R. M., and J. W. Vallance (2001), New views of granular mass flows, *Geology*, *29*(2), 115–118.

Iverson, R. M., M. Logan, and R. P. Denlinger (2004), Granular avalanches across irregular three-dimensional terrain: 2. Experimental tests, *J. Geophys. Res.*, *109*, F01015, doi:10.1029/2003JF000084.

Iverson, R. M., M. Logan, R. G. LaHusen, and M. Berti (2010), The perfect debris flow? Aggregated results from 28 large-scale experiments, *J. Geophys. Res.*, *115*, F03005, doi:10.1029/2009JF001514.

Jain, N., J. M. Ottino, and R. M. Lueptow (2004), Effect of interstitial fluid on granular flowing layer, *J. Fluid Mech.*, *508*, 23–44, doi:10.1017/S0022112004008869.

Liang, Y., J. D. Price, D. A. Wark, and E. B. Watson (2001), Nonlinear pressure diffusion in a porous medium: Approximate solutions with applications to permeability measurements using transient pulse decay method, *J. Geophys. Res.*, *106*, 529–535, doi:10.1029/2000JB900344.

Lorences, M. J., G. S. Patience, F. V. Díez, and J. Coca (2003), Fines effects on collapsing fluidized beds, *Powder Technol.*, *131*, 234–240, doi:10.1016/S0032-5910(03)00004-4.

Major, J. J. (2000), Gravity-driven consolidation of granular slurries: Implications for debris-flow deposition and deposit characteristics, *J. Sediment. Res.*, *70*, 64–83, doi:10.1306/2DC408FF-0E47-11D7-8643000102C1865D.

Major, J. J., and R. M. Iverson (1999), Debris-flow deposition: Effects of pore-fluid pressure and friction concentrated at flow margins, *Geol. Soc. Am. Bull.*, *111*, 1424–1434, doi:10.1130/0016-7606(1999)111<424:DFDEOP>2.3.CO;2.

Major, J. J., R. M. Iverson, D. F. McTigue, S. Macias, and B. K. Fiedorowicz (1997), Geotechnical properties of debris-flow sediments and slurries, paper presented at 1st International Conference, Am. Soc. Civ. Eng., San Francisco, Calif.

McArdell, B. W., P. Bartelt, and J. Kowalski (2007), Field observations of basal forces and fluid pore pressure in a debris flow, *Geophys. Res. Lett.*, *34*, L07406, doi:10.1029/2006GL029183.

McClung, D., and P. Schaerer (1993), *The Avalanche Handbook*, Mountaineers, Seattle, Wash.

Montserrat, S., A. Tamburrino, Y. Niño, and O. Roche (2007), Kinematics and pore pressure dynamics in aerated granular flows, paper presented at 32nd Congress, Int. Assoc. of Hydraulic Eng. and Res., Venice, Italy.

Naef, D., D. Rickenmann, P. Rutschmann, and B. W. McArdell (2006), Comparison of flow resistance relations for debris flows using a one-dimensional finite element simulation model, *Nat. Hazards Earth Syst. Sci.*, *6*, 155–165, doi:10.5194/nhess-6-155-2006.

Patankar, S. (1980), *Numerical Heat Transfer and Fluid Flow*, McGraw Hill, New York.

Pudasaini, S. P., Y. Wang, and K. Hutter (2005), Modeling debris flows down general channels, *Nat. Hazards Earth Syst. Sci.*, *5*, 799–819, doi:10.5194/nhess-5-799-2005.

Richardson, J. F., and W. N. Zaki (1954), Sedimentation and fluidization: Part I, *Trans. Inst. Chem. Eng.*, *32*, 35–52.

Roche, O., M. A. Gilbertson, J. C. Phillips, and R. S. J. Sparks (2004), Experimental study of gas-fluidized granular flows with implications for pyroclastic flows emplacement, *J. Geophys. Res.*, *109*, B10201, doi:10.1029/2003JB002916.

Roche, O., S. Montserrat, Y. Niño, and A. Tamburrino (2008), Experimental observations of water-like behavior of initially fluidized, dam break granular flows and their relevance for the propagation of ash-rich pyroclastic flows, *J. Geophys. Res.*, *113*, B12203, doi:10.1029/2008JB005664.

Roche, O., S. Montserrat, Y. Niño, and A. Tamburrino (2010), Pore fluid pressure and internal kinematics of gravitational laboratory air-particle flows: Insights into the emplacement dynamics of pyroclastic flows, *J. Geophys. Res.*, *115*, B09206, doi:10.1029/2009JB007133.

Savage, S. B., and K. Hutter (1989), The motion of a finite mass of granular material down a rough incline, *J. Fluid Mech.*, *199*, 177–215, doi:10.1017/S0022112089000340.

Savage, S. B., and R. M. Iverson (2003), Surge dynamics coupled to pore-pressure evolution in debris flows, in *Debris-flow Hazard Mitigation: Mechanics, Prediction and Assessment*, edited by D. Rickenman and C. L. Chen, pp. 503–514, Millpress, Rotterdam, Netherlands.

Turnbull, B., and J. N. McElwaine (2007), A comparison of powder snow avalanches at Vallée de la Sionne with plume theories, *J. Glaciol.*, *53*, 30–40, doi:10.3189/172756507781833938.

Versteg, H., and W. Malalasekera (1995), *An Introduction to Computational Fluid Dynamics: The Finite Volume Method*, Wiley, New York.

Vollmöller, P. (2004), A shock-capturing wave-propagation method for dry and saturated granular flows, *J. Comput. Phys.*, *199*, 150–174, doi:10.1016/j.jcp.2004.02.008.

Wilson, C. J. N. (1980), The role of fluidization in the emplacement of pyroclastic flows: An experimental approach, *J. Volcanol. Geotherm. Res.*, *8*, 231–249, doi:10.1016/0377-0273(80)90106-7.

Wilson, L., and J. W. Head (1981) Morphology and rheology of pyroclastic flows and their deposits, and guidelines for future observations, *U.S. Geol. Surv. Prof. Pap.*, *1250*, 513–524.

Yilmaz, O., R. C. Nolen-Hoeksema, and A. Nur (1994), Pore pressure profiles in fractured and compliant rocks, *Geophys. Prospect.*, *42*, 693–714, doi:10.1111/j.1365-2478.1994.tb00236.x.